

Potential Pulsed Electrodeposition of CuInSe₂ Thin Films

A. Burgos^{1,*}, R.S. Schrebler¹, H. Gómez¹, F.A. Cataño¹, R. E. Marotti², E. A. Dalchiele²

¹Instituto de Química, Pontificia Universidad Católica de Valparaíso, Av. Universidad #330, Curauma, Valparaíso, Chile.

²Instituto de Física & CINQUIFIMA, Facultad de Ingeniería, Herrera y Reissig 565, C.C. 30, Montevideo 11000, Uruguay.

*E-mail: anitaester76@gmail.com

Received: 27 August 2015 / Accepted: 2 October 2015 / Published: 4 November 2015

Copper indium diselenide (CISE) thin films have been prepared onto ITO glass substrates by a potential pulsed electrodeposition method from a pH = 3.0 buffer solution containing CuCl₂, InCl₃ and SeO₂ as precursors. After applying a series of potential/time pulsed programs it was possible to find specific potential intervals allowing to growing CISE films whose X-ray diffraction patterns showed single phase polycrystalline chalcopyrite structure. Raman spectra analysis of these as grown films confirmed this finding. From optical measurements a bandgap of 1.01 eV was determined. By recording Mott–Schottky plots it was found that the films presented *p*-type conductivity, a carrier density $N_A = 8.54 \times 10^{19} \text{ cm}^{-3}$ and a flatband potential $E_{FB} = 0.35 \text{ V}$.

Keywords: CISE, potential pulsed electrodeposition, absorber layers, solar cells.

1. INTRODUCTION

CuInSe₂ (CISE), is a chalcopyrite type ternary semiconductor that has attracted considerable attention due to its desirable physical properties [1]. In the field of solar energy conversion the interest lies in the fact that it possesses optimal properties as absorber layer in thin films solar cells [2,3]. It can be obtained under *n* or *p*-type conductivity [4], presents a 1.1 eV direct bandgap and an absorption coefficient of $3 \times 10^4 \text{ cm}^{-1}$ [5]. CISE has been prepared by a variety of methods including electrochemical atomic layer deposition [6,7], chemical vapor deposition [8], co-evaporation, sputtering [9], spray pyrolysis, molecular beam epitaxy [10] and electrodeposition [11,12,13,14]. In particular, electrochemical deposition is well adapted for the development of flexible solar cells as compared with the traditional vapor based deposition methods. Moreover, it is a beneficial technique because of its extensive production possibility, smallest waste of components during process and low

cost [15]. A number of approaches for CISE electrodeposition have been described during the past decade [1, 16, 17], but most of them are limited by the low crystallinity of the as-deposited layers [17] and the incorporation of Se and Cu-Se impurities. To improve the quality of these films, post-deposition treatments that require high temperatures in Se atmosphere and KCN etching have been reported [16,17]. Therefore, the direct electrodeposition of CISE films with a high crystallinity and good stoichiometry still remains a challenge.

Potential pulsed electrodeposition (PPE) appears as an alternative to direct current (dc) potentiostatic or galvanostatic electrochemical methods. This is due to the fact that three independent parameters can be tuned at the same time: potential, period and duty cycle. Setting the amplitude and pulse width it is possible to promote a more controlled nucleus initiation process favoring thus an increase in grain density, resulting in films that present thinner grains with better properties than those prepared by conventional methods [18]. Furthermore, the films present well dispersed deposition and good adherence to the substrate [19]. A number of papers have been devoted to CISE pulsed electrodeposition [1, 20, 21, 22], however most of the as grown films usually are polyphasic requiring a further a post treatment. In current work we report the electrodeposition of CISE absorption layers based on the sequential application of short potential pulses at values settled close to the electroreduction potential of each element, followed by the further solid state reaction when stepping back the potential to start the subsequent sequence of pulses. Different potential pulsed programs impacts on the structural and morphological properties of CISE films and a careful tuning of the pulse parameters allows for obtaining good quality films with optimal thickness at times as short as 200 s.

2. EXPERIMENTAL

The CISE thin films have been electrochemically grown onto transparent electrode substrates consisting of glass plates with a conductive thin film of tin-doped indium oxide ($\text{In}_2\text{O}_3:\text{Sn}$, ITO) on one side (Delta Technologies Limited (USA), sheet resistance of about 5-15 Ω/sq). A typical three electrode electrochemical cell geometry has been used, comprising an ITO substrate (1.0 cm^2), a Pt wire and a silver/silver chloride (Ag/AgCl , $E=0.196 \text{ V}$ vs. NHE) as working, counter and reference electrodes, respectively. All the potentials reported in this study refer to this reference electrode. ITO coated glass substrates were washed with ethanol and thoroughly rinsed with Millipore water, and then dried at $70 \text{ }^\circ\text{C}$ in a controlled atmosphere oven.

CuInSe_2 thin films were cathodically deposited from an aqueous solution containing 4.35 mM $\text{CuCl}_2 + 5.56 \text{ mM InCl}_3 + 8.14 \text{ mM SeO}_2$ dissolved in a $\text{pH} = 3$ lactic/lactate buffer solution employing 0.26 M LiCl as supporting electrolyte. The electrolytic solution was kept at 25°C under argon saturation during all the experiments.

Both, potential pulsed electrochemical depositions and linear sweep voltammograms were carried out by using the same typical three electrode electrochemical cell and electrode materials described above. A potentiostat ZRA SERIES G300 has been used in all these experiments.

To find the crystalline structure of the electrochemical deposited thin films X-ray diffraction patterns were recorded with a Rigaku Ultima diffractometer ($\text{Cu } K_\alpha$, 0.154 nm). A JEOL, JSM 6300

SEM model, was employed to characterize the morphology of the films. The film thickness was measured with a ZEISS, model ULTRA 55, field emission scanning electron microscope (FESEM).

The Raman spectra were recorded on a SNOM/Raman confocal microscope alpha 300 WITEC using a 150 mW laser with a wavelength of 785 nm, 10 accumulations scans 1s integration time.

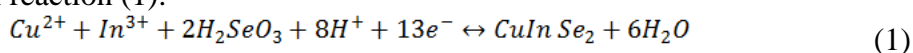
The optical properties were studied using a tungsten lamp source chopped by an SRS SR540 chopper and monochromated by an Oriel 77250 monochromator. The transmitted light was detected with a InGaAs Newport 71616 thermoelectric cooled detector. An SRS SR530 lock-in amplifier extracted the signal from the detector. The ITO coated glass substrate was used as a reference.

Photocurrent measurements were performed forming a semiconductor/electrolyte junction immersing the CISE/ITO glass substrate films in a 0.05 M $\text{Na}_2\text{B}_4\text{O}_7$ (pH=9.3) solution. The light source was a 150 W Xe lamp (ORIEL Instruments 6295 model). The visible light entered the cell through a 0.8 cm^2 quartz window and shined on the film side of the glass. A filter was used in order to remove the ultraviolet radiation. An EG&G APPLIED RESEARCH 273A potentiostat/galvanostat has been employed to carried out these measurements. Mott–Schottky analysis was undertaken by applying a 0.01 Vrms sinusoidal excitation signal with a frequency of 10 kHz by using the same setup. The applied bias ranged from 0.4 to -0.2 V , at a sweeping rate of 0.01 V s^{-1} , sweeping the potential in the negative direction. A 0.1 M tetrabutyl ammonium hexafluorophosphate (TBAPF_6) dissolved in acetonitrile was the electrolytic solution in this case.

3. RESULTS AND DISCUSSION

3.1 Electrochemical study

Figure 1 shows the potentiodynamic j/E curves of an ITO/glass substrate of each solution precursor and their mixtures (Cu(II) + In(III) + Se(IV)), respectively dissolved in a lactic acid/lactate buffer solution. Lactic acid is an alpha carboxylic acid that forms a weak complex with Cu(II) ions, shifting its reduction potential towards more cathodic values bringing it closer to those of the others precursor [1] favoring thus the formation of the CISE phase. Curves **a** to **c** in Figure 1 depicts the electroreduction of the individual Cu (II), In (III) and Se (IV) precursors in this plating bath. A broad current peak with a maximum at -0.29 V (curve **a**) characterizes the electroreduction of Cu (II) to Cu (0), followed by the reduction of Se (IV) to Se (-II) (curve **b**) with a peak potential at -0.94 V . Extending the scan towards more negative potential values starts the In (III) electroreduction (curve **c**). In the presence of all the precursors (curve **d**), appears a current plateau between -0.42 V and -0.80 V . As it has been previously reported in the literature [1] the latter is related to the electroreduction of Se (IV) to Se (-II) which in the presence of Cu(II) and In(III) ions leads to CISE formation trough the overall reaction (1):



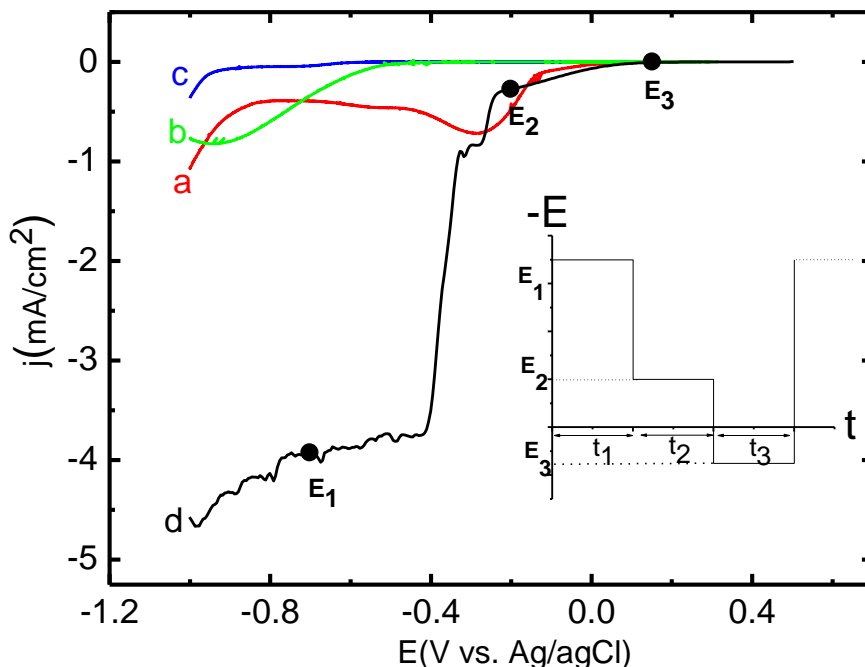


Figure 1. Potentiodynamic j/E curves of an ITO/glass electrode in the following solutions: (a) 4.35 mM CuCl_2 , (b) 8.14 mM SeO_2 , (c) 5.56 mM InCl_3 and (d) 4.35 mM CuCl_2 + 8.14 mM SeO_2 + 5.56 mM InCl_3 + LiCl 0.26 M. In all cases a lactic acid/sodium lactate, pH 3 buffer solution has been used. Scan rate: 10 mVs^{-1} . Inset: typical three step PP waveform perturbation ($E-t$) used during the further electrodeposition of the CISe layer

Taking into account the voltammetric response, potential pulsed programs were designed in order to obtaining CISe films without the presence of not needed phases such as Cu_{2-x}Se which usually requires to be eliminated with a further post annealing treatment. Different electrodeposition potential values and potential pulse sequences were applied in a set of experiments. The inset of Figure 1 shows a typical three step PP waveform perturbation used during the electrodeposition of the CISe layers, a detail of each particular PP programs assayed is described in Table 1. E_1 was set at -0.70 V because at this potential in presence of In(III) take place the reductions of Se(IV) to Se(-II) and Cu(II) to Cu(I) to form the CISe phase [23]. To avoid the presence of elemental copper in the films, E_2 and E_3 were set at potentials where any copper excess is stripped to Cu(II) .

Table 1. Potential, period and duty cycle conditions for CISe electrodeposition.

Program	Pulse potential (V)			Pulse time (s)			Number of cycles
	E_1	E_2	E_3	t_1	t_2	t_3	
PP (I)	-0.70	-0.20	0.15	0.5	0.5	0.5	200
PP (II)	-0.70	-0.20	0.15	1.0	1.0	1.0	100
PP(III)	-0.70	-0.20	---	1.0	1.0	---	100

3.2 Structural and morphological characterization of the films

Figure 2 shows X-ray diffraction patterns corresponding to as deposited CISE films prepared with PP programs I, II and III. Besides the diffraction peaks due to the substrate (marked as “ITO”), diffraction peaks at $2\theta = 26.84^\circ$, 44.42° and 52.44° , corresponding respectively to the (112), (204, 220) and (116, 312) crystallographic planes of the chalcopyrite CISE [24] are present with different intensities in every diffractogram. In general, broad and weak diffraction peaks are present when CISE films were grown employing PP I and PP II programs, instead more intense peaks appear for CISE layers grown by applying PP III program.

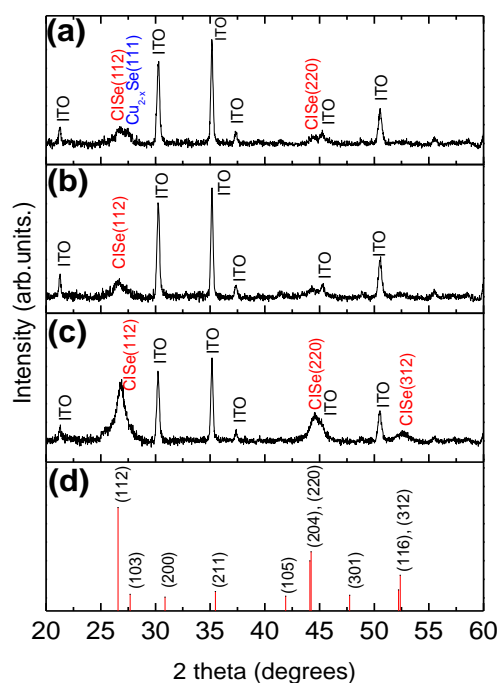


Figure 2. X-ray diffraction patterns of as-grown CISE films onto an ITO/glass substrate by applying different electrodeposition potential pulsed programs: (a) PP (I), (b) PP (II) and (c) PP (III). (ITO indicates the peaks originated from the substrate). (d) Chalcopyrite CISE JCPDS (Card N° 40-1487) pattern is also shown for comparison.

For films grown employing PP (I) program the diffraction peak related to the (112) crystallographic plane appears poorly resolved. The shoulder at $2\theta = 27.34^\circ$ is attributed to the presence of Cu_{2-x}Se as a secondary phase which is probably promoted by the presence of a Se excess in the film [25,11]. Besides, the height of the diffraction peak for planes (204,220) is barely visible, while the corresponding to the (312) plane is absent for layers grown under these conditions.

For a film grown by the PP (II) program the resolution of diffraction peaks is slightly improved, entailing now the lack of the shoulder associated to the Cu_{2-x}Se phase, the rest of the peaks remaining practically unchanged. Applying the PP (III) program results in a diffractogram reflecting a noticeable improving in the structural and crystallographic characteristics of the CISE as deposited films. The three main peaks of the chalcopyrite CISE structure appear well defined and with improved

peak intensities. Comparing the values of the ratio intensity of the diffraction peaks ($I_{(112)}/I_{(220)}=2.3$) to the respective intensity ratio of the JCPDS pattern (1.74), a slightly preferred growth along the (112) plane is expected [14, 21,26,27]. This preferred orientation is desirable in CISe thin films intended for use in solar cells, since then there is the least crystallographic mismatch (ca. 1.1%) with CdS thin film grown on top [14]. On the other hand, the broadening of the diffraction peaks reflects an small crystallite size, in fact the average size calculated from the Scherrer equation [28] from the peak corresponding to the (112) crystallographic plane gave a value of 8.4 nm. The absence of diffraction peaks corresponding to undesired phases relieves the importance of a proper design of the potential pulse parameters for achieving good quality as deposited CISe films.

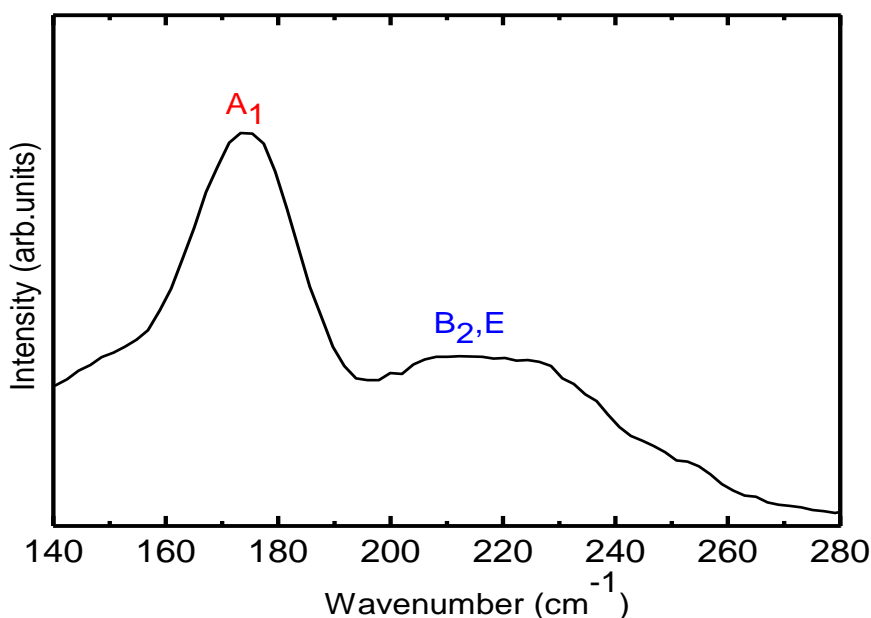


Figure 3. Raman spectra of CISe samples prepared by applying pulsed program PP (III).

Raman spectroscopy has been extensively employed to characterize the composition of electrodeposited CISe thin films [29]. Figure 3 display the Raman spectrum in the range between 140-280 cm^{-1} for a CIS film electrodeposited applying the PP (III) program. The main peak at 173.9 cm^{-1} corresponds to the A_1 vibrational mode which is close to the accepted value for the CuInSe_2 chalcopyrite crystallographic structure [30]. The position of the peak can appear slightly shifted towards the blue as compared with the reported value for the chalcopyrite CuInSe_2 crystallographic structure (173 cm^{-1}) [31] Between 200-230 cm^{-1} is observed a band of low intensity associated to the B_2,E vibrational mode, attributed to the Cu-In bonds vibrations [21].

As is shown in Figure 4, the morphology of the electrodeposited films is also dependent on the type of pulse program employed. For I and II PP programs (Figure 4a and 4b), the films are porous and exhibit agglomerates spread over the entire surface with irregular size grains. However, by employing PP program III (Figure 4c), homogeneous and compact films with uniform size grains are obtained. A

thickness of 1.78 μm has been determined from a cross section image of these films (Figure 4d), a value well adapted to the requirements needed for the absorber layers in photovoltaic devices [32].

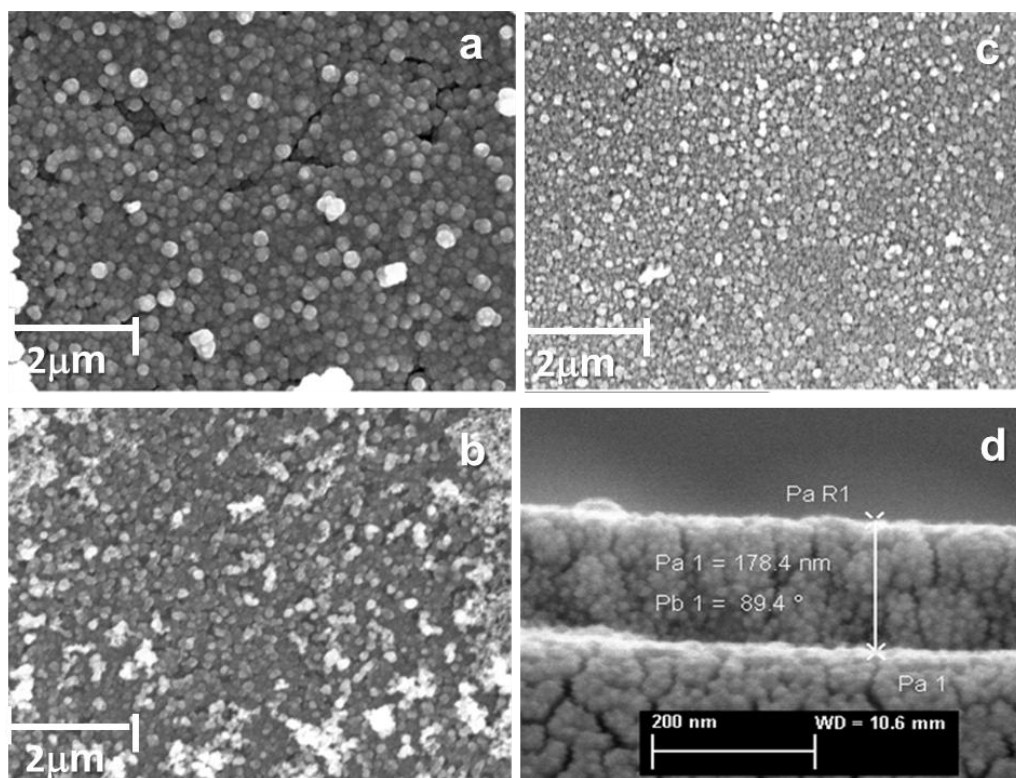


Figure 4. Surface view SEM images of typical electrodeposited CISE films onto an ITO/glass substrate by applying different electrodeposition potential pulsed programs: (a) PP (I), (b) PP (II) and (c) PP (III). (d) Cross sectional view of a CISE layer obtained under PP (III) program.

3.3 Optical characterization

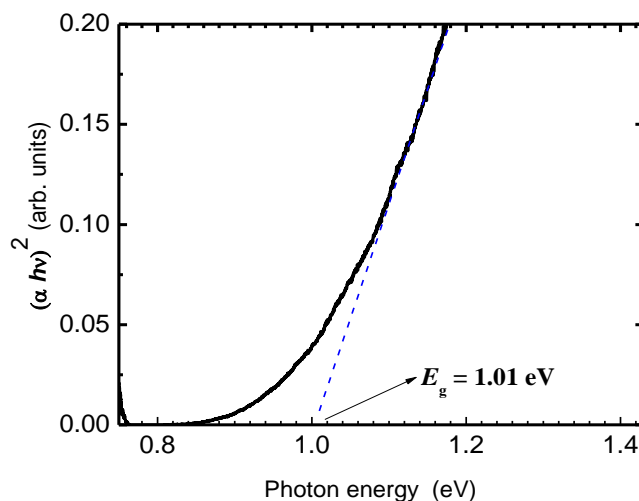


Figure 5. NIR Tauc plot for direct allowed band-gap of electrochemically as-grown CISE film onto an ITO/glass substrate by applying electrodeposition potential pulsed programs PP (III).

The bandgap energy values (E_g) of the semiconductor films were determined from transmittance spectra of the films obtained applying PP program III by using the well known Tauc relation in (2):

$$\alpha h\nu = A(h\nu - E_g)^n \tag{2}$$

Where A is a constant, $h\nu$ is the photon energy, α is the absorption coefficient, and n depends on the nature of the transition. For direct allowed transitions $n = \frac{1}{2}$ [33]. Therefore in a plot of $(\alpha h\nu)^2$ vs $h\nu$, the E_g value can be found by extrapolating the linear portion of the plot to the energy axis at $\alpha = 0$ [34] as shown in Figure 5. In this curve the $\alpha = 0$ line was corrected for any residual sub-bandgap absorption or light dispersion (by an indirect like absorption profile, i. e. $n = 2$ in equation (2)) [35]. From the linear fitting showed in Figure 5, an E_g value of 1.01 eV has been obtained, which agrees well with those reported in the literature for the CISE phase [8, 36, 20, 37].

3.4 Photoelectrochemical characterization

The semiconducting properties of ternary chalcopyrite compounds depend on their non-stoichiometry and are related to the presence of intrinsic defects such vacancies and interstitials. The semiconductor properties of the CISE films were studied employing electrochemical impedance spectroscopy measurements. The analysis of the interfacial capacitance vs potential data were analyzed from the Mott–Schottky equation, written as [38]:

$$\frac{1}{C^2} = \left(\frac{2}{e\epsilon_r\epsilon_0NA^2} \right) \left(V - V_{FB} - \frac{kT}{e} \right) \tag{3}$$

where C is the differential capacitance of the space-charge region, ϵ_0 , the permittivity of vacuum, ϵ_r the relative dielectric constant, N the donor carrier density for n-type semiconductor or the acceptor carrier density for a p-type semiconductor, A the surface area of the sample, V the electrode potential, and V_{FB} the flatband potential.

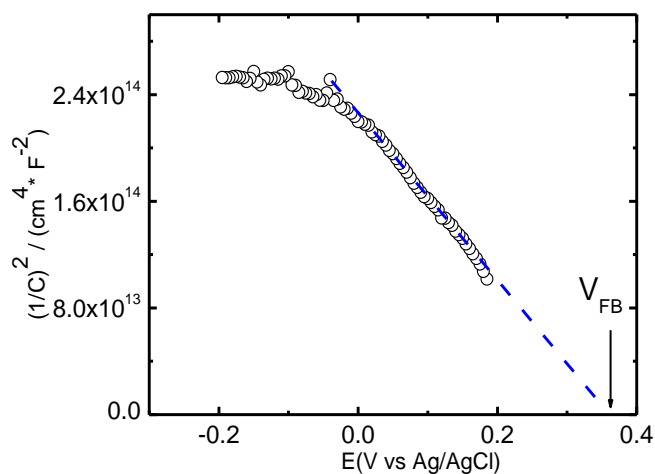


Figure 6. C^{-2}/E (Mott-Schottky) plot for a CISE/ITO glass substrate electrode measured at 10 kHz under dark conditions. The CISE layer has been grown by the electrodeposition program PP (III). Electrolyte solution: 0.1 M (TBAPF₆) in acetonitrile. Actual data (circles), linear fittings (dashed line). The flat band potential is also indicated.

The dielectric constant ϵ is taken as 10 [39]. Figure 6 shows the plot of the inverse of the square of the capacitance as function of the electrochemical potential of a sample prepared by PP (III) electrodeposition program. As predicted by the Mott–Schottky equation a linear relationship with a negative slope is obtained, confirming that the CISe layer presents the semiconductor characteristic of a p-type material. The intercept on the applied potential axis yields 0.35 V for the flat band potential. The acceptor carrier concentration (N), calculated from the slope, resulted in $8.54 \times 10^{19} \text{ cm}^{-3}$. This acceptor carrier concentration is higher than expected, but it is important to highlight that most of the data in the literature correspond either to ingots [40] or monocrystalline materials [39]. The presence of grain borders and surface states can increase noticeably [21] the number of defects in the films, being these the reasons why similar high values of carrier density in electrodeposited CISe films has been reported [41].

The photoelectrochemical performance of the electrochemically grown CISe layers has been explored using a liquid-junction in a photoelectrochemical system under white illumination for films obtained with the PP (III) electrodeposition program. A semiconductor electrode should to show rectifying behavior under the polarization regime corresponding to minority carrier current flow. It is expected that for a p-type material rectification be observed at potentials negative of the flatband value. Under illumination electron and holes are separated in the space charge region and further driven in opposite directions by the effect of the electric field. The p-type conductivity of CISe predicts the apparition of a negative photocurrent as result of the migration of electrons towards the electrode/electrolyte interface increasing then the cathodic current.

Figure 7 shows current density–potential j/E potentiodynamic responses for the CISe/ITO glass substrate electrode under different experimental conditions: in darkness, under illumination, and under chopped light conditions. The dark current density (J_d) is small (-0.025 mA) which means that CISe forms a blocking contact with the electrolyte. Under irradiation, appears a cathodic photocurrent J_{ph} indicating that the film presents a p-type character. The onset of the photocurrent is in good agreement with the flat band potential that can be derived from the Mott-Schottky plot ($E_{FB} = 0.35 \text{ V vs. SCE}$) according to the relation that $J_{ph} \propto (V_{FB} + V)$ [41].

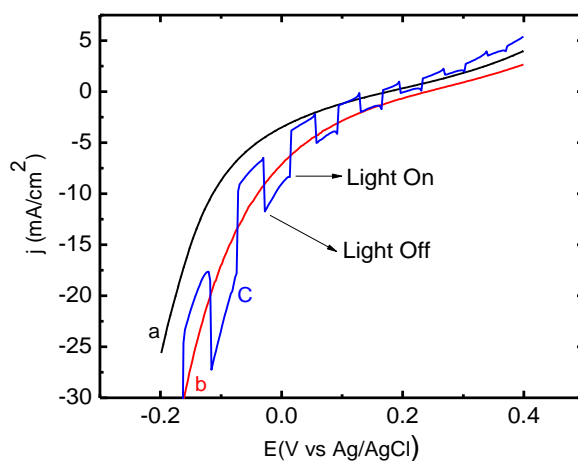


Figure 7. j/E response curves for a CISe film grown with a PP (III) programa: (a) in the dark; (b) under continuous white illumination; (c) with chopped white light. Electrolyte: 0.05 M $\text{Na}_2\text{B}_4\text{O}_7$, pH = 9.3. Scan rate 10 mVs^{-1} . Light intensity 100 mWcm^{-2} .

4. CONCLUSIONS

CuInSe₂ films were electrodeposited onto ITO glass at room temperature from a single bath by applying different potential pulsed programs. Specific pulsed programs lead to obtain CISE films with good morphological, stoichiometric and structural properties without the presence of secondary phases. The as grown samples are oriented along the (112) crystallographic direction, further annealing would be required for improving the crystallite sizes for application as absorber layer in thin film solar cells. The diffusion condition established by applying the potential pulse programs accounts for the differences in morphology and composition. Photoelectrochemical measurements, and Mott-Schottky plots confirmed p-type conductivity. Besides, together with absorption spectra it was possible to evaluate relevant optoelectronic properties for this semiconductor, such as band gap energy, flat band potential and acceptor carrier concentration.

ACKNOWLEDGEMENTS

A.B. acknowledge CONICYT (Comisión Nacional de Investigación Científica y Tecnológica de Chile) for the doctoral scholarship awarded and Project Apoyo de Tesis Doctoral grant 24121049. H.G. and R.S. acknowledge European Commission through NanoCIS project FP7-PEOPLE-2010-IRSES grant 269279. EAD and REM thank to CSIC (Comisión Sectorial de Investigación Científica) of the Universidad de la República, Montevideo, Uruguay, PEDECIBA – Física, ANII (Agencia Nacional de Investigación e Innovación), Uruguay FIC Regional CONICYT programs EQU 0003 and FONDEQUIP EQM130170 are also gratefully acknowledged.

References

1. F. Kang, J. Ao, G. Sun, Q. He, Y. Sun, *Mater. Chem. Phys.*, 115 (2009) 516.
2. B. Yin, C. Lou, *Adv. Condens. Matter Phys.*, 2015 (2015) 1.
3. M. Dehghani, A. Behjat, F. Tajabadi, N. Taghavinia, *J. Phys. D: Appl. Phys.*, 48 (2015) 115304.
4. P. Gorley, V. Khomyak, Y. Vorobier, J. González-Hernández, P. Horley, O. Galoshkina, *Sol. Energy*, 82 (2008) 100.
5. J. Araujo, R. Ortíz, A. López-Rivera, J. Ortega, M. Montilla, D. Alarcón, *J. Solid State Electrochem.*, 11 (2007) 407.
6. H. Kou, X. Zhang, Y. Jiang, J. Li, S. Yu, Z. Zheng, C. Wang, *Electrochim. Acta*, 56 (2011) 5575.
7. D. Banga, N. Jarayaju, L. Sheridan, Y. Kim, B. Perdue, X. Zhang, Q. Zhang, J. Stickney, *Langmuir*, 28 (2012) 3024.
8. M. Berruet, W. Schreiner, S. Ceré, M. Vázquez, *J. Alloys Compd.*, 509 (2011) 3019.
9. J. Bekker, *Sol. Energy Mater. Sol. Cells*, 93 (2009) 539.
10. J. Eberhardt, K. Schulz, H. Metzner, J. Cieslak, Th. Hahn, U. Reislöhner, M. Gossla, F. Hudert, R. Goldhahn, W. Witthuhn, *Thin Solid Films*, 515 (2007) 6147.
11. S. Kang, Y. Kim, D. Choi, Y. Sung, *Electrochim. Acta*, 51 (2006) 4433.
12. N. Chaure, J. Young, A. Samantilleke, I. Dharmadasa, *Sol. Energy Mater. Sol. Cells*, 81 (2004) 125.
13. H. Gómez, R. Schrebler, L. Basáez, E. Dalchiele, *J. Phys.: Condens. Matter*, 5 (1993) A349.
14. R. Ugarte, R. Schrebler, R. Cordova, E. Dalchiele, H. Gomez, *Thin Solid Films*, 340 (1999) 117.
15. C. Huang, T. Meen, M. Lai, W. Chen, *Sol. Energy Mater. Sol. Cells*, 82 (2004) 553.
16. E. Saucedo, V. Izquierdo-Roca, C. Ruiz, L. Parissi, C. Broussillou, P. Grand, J. Jaime-Ferrer, A. Pérez-Rodríguez, J. Morante, V. Bermúdez, *Thin Solid Films*, 517 (2008) 2268.

17. J. Wellings, A. Samantilleke, S. Heavens, O. Warren, I. Dharmadasa, *Sol. Energy Mater. Sol. Cells*, 93 (2009) 1518.
18. M. Chandrasekar, M. Pushpavanam, *Electrochim. Acta*, 53 (2008) 3313.
19. T. Edamura, J. Muto, *J. Mater. Sci. - Mater. Electron.*, 5 (1994) 275.
20. A. Palacios-Adrós, F. Caballero-Briones, Fausto Sanz, *Electrochem. Commun.*, 12 (2010) 1025.
21. M.H. Valdés, M. Vázquez, *Electrochim. Acta*, 56 (2011) 6866.
22. N. Ghamarian, Z. Zain, M. Zidan, W. T. Tan, *Int. J. Electrochem. Sci.*, 8 (2013) 312.
23. D. Lincot, J. Guillemoles, S. Taunier, D. Guimard, J. Sicx-Kurdi, A. Chaumont, O. Roussel, O. Ramdani, C. Hubert, J. Fauvarque, N. Bodereau, L. Parissi, P. Panheleux, P. Fanouillere, N. Naghavi, P. Grand, M. Benfarah, P. Mogensen, O. Kerrec, *Sol. Energy*, 77 (2004) 725.
24. Database: Joint Committee on Powder Diffraction- International Centre for Diffraction Data (JCPDS-ICDD). JCPDS, Card No 40-1487. (<http://www.icdd.com>).
25. M. Calixto, K. Dobson, B. McCandless, R. Birkmire, *J. Electrochem. Soc.*, 153 (2006) 521.
26. J. Li, X. Zhao, D. Xia, *J. of Wuhan University of Technol.-Mater.*, 22 (2006) 140.
27. C. Sene, M. Calixto, K. Dobson, R. Birkmire, *Thin Solid Films*, 516 (2008) 2188.
28. B.D. Cullity, *Elements of X-ray Diffraction*. Massachusetts, U.S.A. (1978).
29. O. Roussel, O. Ramdani, E. Chassaing, P. Grand, M. Lamirand, A. Etcheberry, O. Kerrec, J. Guillemoles, D. Lincot, *J. Electrochem. Soc.*, 155 (2008) D141.
30. V. Izquierdo-Roca, A. Pérez-Rodríguez, A. Romano-Rodríguez, J.R. Morante, J. Alvarez-García, L. Calvo-Barrio, V. Bermudez, P.P. Grand, O. Ramdani, L. Parissi, O. Kerrec, *J. Appl. Phys.* 101 (2007) 103517.
31. C-S. Chiang, W. Lee, T. Chang, Y. Su, *J. Appl. Electrochem.*, 45 (2015) 549].
32. J. Pettersson, T. Torndahl, C. Platzer-Björkman, A. Hultqvist, M. Edoff, *IEEE J. of photovoltaics*, 3 (2013) 1376.
33. S. Prabahar, V. Balasubramanian, N. Suryanarayanan, N. Muthukumarasamy. *Thin films Chalcogenide*, 7 (2010) 49.
34. C. Chavhan, R. Sharma, *Phys. Chem. solids*, 67 (2006) 767.
35. C. Pereyra, R. Marotti, G. Guerguerian, F. Elhordoy, L. Campo, L. Amy, D. Gau, F. Martín, D. Leinen, J. Ramos-Barrado, E. Dalchiele. *Energy and Environ. Focus*, 2 (2013) 257.
36. O. Meglali, A. Bouraiou, N. Attaf. *Rev. des Energies Renouvelables*, 11 (2008) 19.
37. A. Shanmugavel, K. Srinivasan, K. R. Murali. *J. Mater. Sci.: Mater. Electron*, 24 (2013) 2398.
38. E. Hernández-Pagán, W. Wang, T. Mallouk. *ACS Nano*. 5 (2011) 3237.
39. H. Du, C. Champness, I. Shih. *Thin solid films*. 480-481 (2005) 37.
40. L. Djellal, A. Bouguelia, M. Trari. *Mater. Chem. Phys.* 109 (2008) 99.
41. R. Raffaele, H. Forsell, T. Potdevin, R. Friedfeld, J. Mantovani, S. Bailey, S. Hubbard, E. Gordon, A. Hepp. *Sol. Energy Mater.*, 57 (1999) 167.